Inverse mapping of block copolymer morphologies

Lyakhova, K.; Zvelindovsky, A.V.; Sevink, G.J.A.; Fraaije, J.G.E.M.

Inverse mapping of block copolymer morphologies

K. S. Lyakhova, A. V. Zvelindovsky, G. J. A. Sevink, and J. G. E. M. Fraaije

Citation: The Journal of Chemical Physics **118**, 8456 (2003); doi: 10.1063/1.1565328
View online: https://doi.org/10.1063/1.1565328
View Table of Contents: http://aip.scitation.org/toc/jcp/118/18
Published by the American Institute of Physics

Inverse mapping of block copolymer morphologies

K. S. Lyakhova, A. V. Zvelindovsky, G. J. A. Sevink, and J. G. E. M. Fraaije
Leiden Institute of Chemistry, University of Leiden, Einsteinweg 55, P.O. Box 9502 2300, RA Leiden, The Netherlands

(Received 13 June 2002; accepted 11 February 2003)

Polymer morphologies can be analyzed by various experimental projection methods. Since most structures live in three dimensions the problem is to extrapolate the underlying 3D morphology from the projection. We propose an approach in which the free energy functional of a 3D sample is minimized to fit experimental 2D information, serving as an additional constraint. The method is very general and can be applied to any physical system described in terms of a density functional theory. © *2003 American Institute of Physics.* [DOI: 10.1063/1.1565328]

I. INTRODUCTION

Morphological structures in block copolymer melts, blends and concentrated solutions are receiving increasing attention.[1–3] In the area of block copolymer melts and solutions, there is a limited number of methods to reconstruct bulk three-dimensional (3D) morphologies from experimental series of 2D density profiles, such as electron microscopy, atomic force microscopy,[4] and laser scanning confocal microscopy.[5] In this paper we propose a generally applicable *inverse mapping* theory for refinement and extension of the experimental reconstructions. To demonstrate the principle we carry out a series of toy simulations in lower dimensional systems (1D and 2D), and conclude with realistic calculations for a defected lamelar 3D system, and recent experimental observations from the Bayreuth group on defected cylindrical phases in thin films.[6]

From a theoretical point of view, the problem of reconstructing of volume structures from 2D images was addressed some time ago in stereology. The stereological technique deals, for example, with the derivation of information on the bulk of an ensemble of isotropically arranged monodisperse objects from measurements made on the cross section through the ensemble.[7,8] However, experimental structures of block copolymer systems often are far from perfect. Rather, the key novelty in our method is to combine a proper free energy functional for polymer system directly with the experimental data. The method does not restrict the symmetry of the system, nor does it require a perfect geometry: it is soft and flexible.

II. THEORY

The block copolymer melt is modeled as a system of Gaussian chain molecules in a mean field environment. The free energy functional is[9–11]

$$F[\rho]=-kT\ln\frac{\Phi^n}{n!}-\sum_{I\in\mathbf{S}}\int_V U_I(\mathbf{r})\rho_I(\mathbf{r})d\mathbf{r}+F^{\mathrm{nid}}[\rho], \quad (1)$$

where n is the number of polymer molecules, Φ is the intramolecular partition function for ideal Gaussian chains, I is an index for S components ($\mathbf{S}=\{1,\ldots,S\}$) and V is the system volume. The external potentials U_I are conjugate to the densities ρ_I via the Gaussian chain density functional.[9] The nonideal free energy F^{nid} describes the mean-field interaction between chemically different blocks.[10] In thermodynamic equilibrium, the morphology is implicitly determined by the self-consistent-field condition $\mu_I\equiv\delta F/\delta\rho_I=0$ with $F_{\rho\rho}>0$. In the usual case there are many such equilibria, each corresponding to a different metastable morphology.

We include the experimental constraining field by following the method of Lagrange.[12] We suppose that in a certain domain $\Omega\subseteq V$ the densities ρ_I^0 of the components I in the subset $\mathbf{s}$ ($\mathbf{s}\subseteq\mathbf{S}$) are known. The constraining functional is

$$E=\sum_{I\in\mathbf{s}}\int_\Omega\lambda_I(\mathbf{r})[\rho_I(\mathbf{r})-\rho_I^0(\mathbf{r})]d\mathbf{r}, \quad (2)$$

where λ_I is the Lagrange multiplier field for the Ith component.

The mathematical problem is reduced to finding the extremum of $R=F+E$, such that $R_{\rho_I}\equiv\delta R/\delta\rho_I=0$ and $R_{\lambda_I}=\delta R/\delta\lambda_I=0$, by variation of both $\rho_I(\mathbf{r})$ and $\lambda_I(\mathbf{r})$. The determinant $R_{\rho\rho}R_{\lambda\lambda}-R_{\rho\lambda}^2=-R_{\rho\lambda}^2$ is negative and hence the extremum is a saddle point in $\{\rho,\lambda\}$ space—this is a fundamental property of the Lagrange method. If the saddle point coincides with the true equilibrium $\mu_I=0$, the Lagrange multiplier field is zero too ($\lambda_I=0$), otherwise the Lagrange multiplier field will have a finite value. One can give a physical interpretation to λ_I, such as a selective pressure field which forces the component I in the desired morphology in the domain Ω. However, we believe that physical nature should be determined by the experimental environment, when such field cannot physically be present, λ_I is simply a mathematical artifice.

In the spirit of earlier work the extremum of R is found in a quasidynamical fashion, by adaption of the external potential dynamics algorithms.[13] An equation of motion for the auxiliary field U_I is derived from the collective dynamics of concentration fields ρ_I; for propagation of the λ_I the equation that corresponds to the dynamics of nonconserving property,

$$\frac{\partial U_I}{\partial\tau}+M_I^\rho\Delta R_{\rho_I}+\eta_I=0, \quad (3)$$

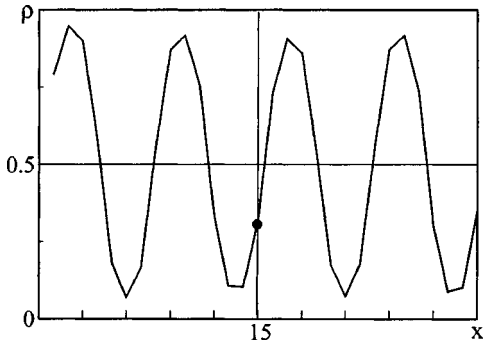

FIG. 1. Density profile of the A_8B_8 block copolymer with fixed density of the A component in the point $x_0=15$ (shown as a dot).

$$\frac{\partial \lambda_I}{\partial \tau} - M_I^{\lambda} R_{\lambda_I} + \eta_I^{\lambda} = 0, \tag{4}$$

where $M_I^{(\rho,\lambda)}$ is a positive mobility coefficient, and $\eta_I^{(\rho,\lambda)}$ is a small random field (white noise). The random field is not essential, but it helps in small barrier crossings. The constrained intrinsic chemical potential is $R_{\rho_I} \equiv \delta R/\delta \rho_I = \mu_I + \omega \lambda_I$, with $\omega > 0$ a shape field determined by the domain Ω, and the constraining potential is $R_{\lambda_I} \equiv \delta R/\delta \lambda_I = \omega(\rho_I - \rho_I^0)$. The dynamical equation for λ_I does not in any way suggest a model for a physically realistic process. Here, it is merely a convenient numerical technique for finding the solution for a very large set of nonlinear equations.

III. STABILITY ANALYSIS

We limit the analysis to a one-component system, omit the noise, and use compact symbolic notation for spatial operator products. The relaxation matrix of the dynamical system is

$$\begin{pmatrix} M^{\rho} \Delta P F_{\rho\rho} & -M^{\rho} \Delta R_{\rho\lambda} \\ -M^{\lambda} P R_{\lambda\rho} & 0 \end{pmatrix}, \tag{5}$$

where we have used $R_{\rho U} = -PR_{\rho\rho} = -PF_{\rho\rho}$, with P the polymer correlation matrix $P \equiv -\delta\rho/\delta U > 0$. All eigenvalues are negative when the saddle point coincides with a minimum in the free energy ($F_{\rho\rho} > 0$): the saddle point is then a stable stationary point in the time-iteration. If the saddle point coincides with an unstable point of the free energy (at least one eigenvalue of $F_{\rho\rho}$ negative), the system of equations may diverge in pathological cases. It is rather cumbersome to find an exact measure for such behavior from the stability analysis; there is a bit of trial-and-error inherent in selecting the proper values for mobility coefficients and free energy parameters. In practice we have found that with $M^{\lambda} \ll M^{\rho}$ the system also converges when the Lagrange multiplier fields remain within reasonable limits, corresponding to roughly the thermal energy kT per computational cell.

By construction of R and the quasidynamical equations, nothing definite can be said about the sign of the time-evolution of R or F. During the course of the iteration both may go up and down—indeed they should have precisely this behavior, since the starting configuration may either be below or above the saddle point. This is in contrast to the original external potentials algorithm which guarantees a decrease in free energy always.

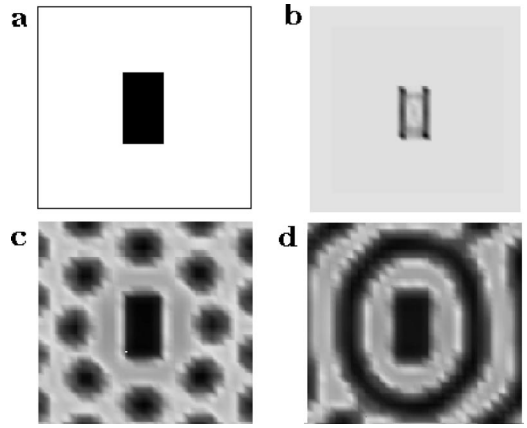

FIG. 2. For the time step $\tau = 500$ in the 2D box: (a) the constraining mask: $\rho_A^0 = 0.9$ in a black rectangle; (b) λ field for the A_8B_8 block copolymer; (c) morphology for the A_6B_{10} block copolymer; (d) morphology for the A_8B_8 block copolymer.

IV. DEMONSTRATION: TOY PROBLEMS

We first discuss a few simple examples of constrained diblock polymer phases in 1D, 2D, and 3D. For all these simulations the Flory–Huggins parameter was chosen as $\chi N = 20$, slightly above the order–disorder transition. The other numerical parameters and integration method are as we used before,[9] with $M^{\rho} = 1$ and $M^{\lambda} = 0.05$.

(1D) Polymer A_8B_8 on a line of 30 grid points with periodic boundary conditions. In the middle of the line the density of the A component is fixed ($\rho_A^0(x_0 = 15) = 0.2$), and the proper constraining field λ (which is in this case only one scalar) and concentration fields ρ_I are calculated. The position of the constrained value of the A component is denoted as a black dot on the slope of the oscillatory density profile in Fig. 1.

(2D) Polymers A_6B_{10} and A_8B_8 in a rectangular box (30×30) with constraining mask—a rectangle of 4×8 grid points. Inside of the rectangle the concentration of the A component is constrained to $\rho_A^0 = 0.9$. The system outside of rectangle is free of any constraints, see Fig. 2. The symmetric polymer forms perturbed lamellae, and the asymmetric

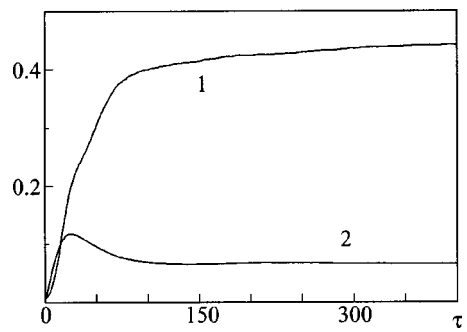

FIG. 3. The time evolution of the order parameter P (1) and the L_2 norm of Lagrange multiplier λ (2) for the A_8B_8 block copolymer [see Fig. 2(d)].

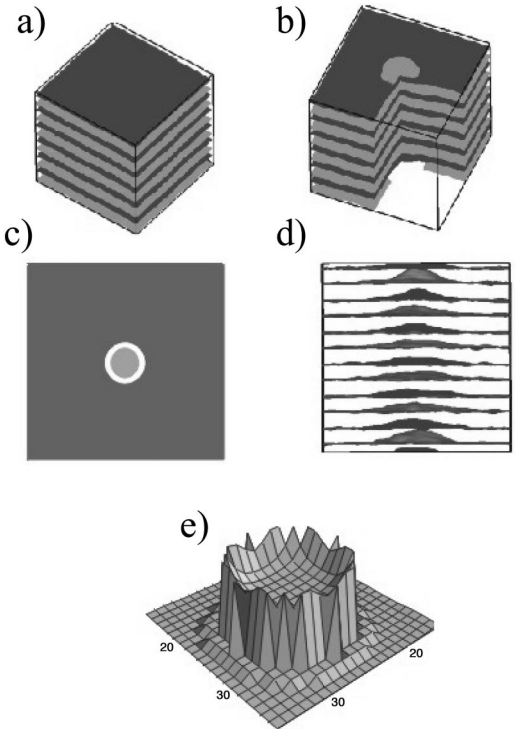

FIG. 4. Simulation of the A_7B_9 block copolymer in the 3D box with the 2D constraint in a top layer. (a) Isosurface for density of A-beads for the case when a plane with uniform density serves as a constraint; (b) Isosurface for density of A-beads for the case when a uniform density of the constraint contains a hole; (c) constraint with hole; (d) defect propagation in a bulk for (b); (e) λ field at the constraint plane. (Isodensity level is 0.5.)

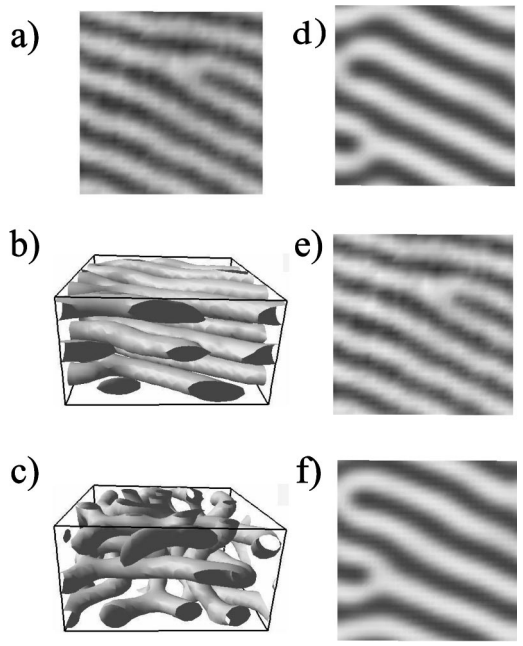

FIG. 5. The $A_3B_{12}A_3$ triblock copolymer in 3D box with experimental data serving as a constraint. (a) The scaled experimental image used as a constraint; (b) Isosurface for the $A_3B_{12}A_3$ block copolymer with constraint at $z=10$. (c) simulation without constraint; (d),(e),(f) the slices through the middle of the layers of cylinders from (b). (Isodensity level 0.5; $\tau=5000$.)

polymer 2D micelles. Figure 3 shows the time evolution of the order parameter for the A component $P=(\rho_A-\overline{\rho_A})^2$ and the norm of Lagrange multiplier field ($\lambda=||\lambda(x,y)||_2$) for the symmetric case of Fig. 2(d). The constraining field λ is 0 at the beginning of calculation. Since the constrained rectangle is not a natural morphology of this particular polymer system, the stationary value of λ is nonzero.

(3D) Polymer A_7B_9 in a box of $51\times51\times51$ grid points. First we fixed in the xy plane at $z=1$ the density of component A to $\rho_A^0=0.99$, and left the remainder of the box unconstrained. The final state is a perfectly lamellar structure [Fig. 4(a)]; this is a true free energy minimum of the system. In reality such lamellar systems often contain defects or undulations. Likewise, 2D images of such lamellar systems contain holes. With the method presented here, we can study the influence of the undulations on the underlying 3D morphology. In order to do this we performed the simulation using a single lamella with a hole defect as a constraint in the first layer [Fig. 4(b)]. In this case an artificial set of experimental data $\rho^0(x,y)$ was used to constrain on the xy plane at $z=1$. The constraining field consists of a lamellar structure with a hole defect. The circles that make up the hole are centered around the midpoint $x=y=25$ and $z=1$. The inner circle has a radius $r_1=6$; the radius of the outer circle $r_2=8$. The concentration is constrained to $\rho_A^0(0<r<r_1)=0.01$ and $\rho_A^0(r>r_2)=0.99$. The system is unconstrained in the ring between r_1 and r_2 and in the remainder of the box. The schematic overview of the constraint is presented in Fig. 4(c).

From Fig. 4(d) one clearly sees how the defect carries through the whole box. The block copolymer still forms a lamellar structure but because of the undulation in the constraint surface, adjacent parallel lamellae possess hole defects as well. In Fig. 4(e) the spatial distribution of the λ field is shown. Since the constraint is confined to the first layer $z=1$, λ is only defined in this layer; λ is also undefined in the unconstrained open part between the inner and outer circle [in Fig. 4(e) λ is given the value zero in this region for visualization purposes]. The Lagrange multiplier field is negative in the outer region ($\rho_A=0.99$) and positive in the inner region ($\rho_A=0.01$), reflecting the additional potential which a hole defect brings to the system. On the edges of the constraint region the field has wiggly wings; these intricate effects are related to the mathematical properties of the inverse polymer density functional.

V. DEMONSTRATION: AN EXPERIMENTAL SYSTEM

The important application of the presented method is the reconstruction of 3D structures of block copolymers from a set of 2D experimental data. Figure 5(a) shows an example of such experimental image of a cylinder forming system obtained by TM-AFM,[6] a thin film of *polystyrene–block–butadiene–block–polystyrene* (SBS) triblock copolymer. A simulation was done in a box $32\times32\times20$ with the experimental image as a constraint and the block copolymer modeled as a Gaussian chain $A_3B_{12}A_3$.[14] The experimental data were laterally scaled to match the microdomain distances of the experiments and simulations and were positioned in the

middle of the simulation box ($z=10$). The final 3D structure is presented in Fig. 5(b); in Figs. 5(d)–5(f) slices through the middle of the layers of the cylinders are shown. One can see that the cylinders in the system with the constraint are situated in layers while the unconstrained system [Fig. 5(c)] has random orientation of cylinders. The slice through the middle layer is identical to the constraint structure while the layers above and beneath the constraint layer contain defects which are rather symmetrical.

VI. DISCUSSION

An important question is the uniqueness of the predicted morphology. In the general case the information enhanced self-consistent-field equations have many solutions. However, a few interesting limits are apparent: (a) When the system is highly symmetrical the symmetry can impose uniqueness (Fig. 4). In experimental system this might be the case when one measures a slice through a perfect domain structure, for example. (b) When multiple constraints are included, each such constraint will reduce the space of solutions. Clearly, in the limit where a 3D experimental image is used as a constraint, the equations have only one solution, namely the constraint itself. The method is powerful, but must be used with care, and the predictions are more accurate given a realistic molecular model and an experimental image of high symmetry.

VII. CONCLUSIONS

In this paper we have introduced a method for the simulations of a bulk structure of block copolymers with given constraining condition at a lower dimensional hypersurface. The method is able to illustrate the extent of surface defects in the bulk. The method can be used ''to grow'' observed experimental data into three dimensions. The method is very general and can be applied to any physical system described in terms of a density functional theory.

ACKNOWLEDGMENTS

The authors thank A. Knoll, R. Magerle, and G. Krausch (University Bayreuth, Germany) for providing us with the experimental data. The authors also thank the NWO-DFG bilateral program for financial support.

[1] F. Bates and G. Fredrickson, Phys. Today **52**, 32 (1999).
[2] M. Matsen, Curr. Opin. Colloid Interface Sci. **3**, 40 (1998).
[3] H. Kodama and M. Doi, Macromolecules **29**, 2652 (1996).
[4] R. Magerle, Phys. Rev. Lett. **85**, 2749 (2000).
[5] H. Takeno, M. Iwata, M. Takenaka, and T. Hashimoto, Macromolecules **33**, 9657 (2000).
[6] A. Knoll, R. Magerle, and G. Krausch, Macromolecules **34**, 4159 (2001).
[7] D.R. Wilkinson and S. F. Edwards, J. Phys. D **15**, 551 (1982).
[8] R.B.S. Oakeshott and S. F. Edwards, Physica A **189**, 208 (1992).
[9] J. G. E. M. Fraaije, B. A. C. van Vlimmeren, N. M. Maurits, M. Postma, O. A. Evers, C. Hoffmann, P. Altevogt, and G. Goldbeck-Wood, J. Chem. Phys. **106**, 4260 (1997).
[10] N. M. Maurits, B. A. C. van Vlimmeren, and J. G. E. M. Fraaije, Phys. Rev. E **56**, 816 (1997).
[11] B. A. C. van Vlimmeren, N. M. Maurits, A. V. Zvelindovsky, G. J. A. Sevink, and J. G. E. M. Fraaije, Macromolecules **32**, 646 (1999).
[12] G. Korn and T. Korn, *Mathematical Handbook for Scientists and Engineers* (McGraw–Hill, New York, 1961).
[13] N. M. Maurits and J. G. E. M. Fraaije, J. Chem. Phys. **15**, 5879 (1997).
[14] A. Knoll, A. Horvat, K. S. Lyakhova, G. Krausch, G. J. A. Sevink, A. V. Zvelindovsky, and R. Magerle, Phys. Rev. Lett. **89**, 035501 (2002).